Impact of the Oxide Aperture Width on the Degradation of 845 Nm VCSELs for Silicon Photonics

Michele Zenari, Matteo Buffolo, *Member, IEEE*, Fabiana Rampazzo, Carlo De Santi, *Member, IEEE*, Francesca Rossi, Laura Lazzarini, Jeroen Goyvaerts, Alexander Grabowski, Johan S. Gustavsson, Roel Baets, *Life Fellow, IEEE*, Anders Larsson, *Life Fellow, IEEE*, Günther Roelkens, *Senior Member, IEEE*, Gaudenzio Meneghesso, *Fellow, IEEE*, Enrico Zanoni, *Life Fellow, IEEE*, and Matteo Meneghini, *Senior Member, IEEE*

***Abstract*—For the first time, we analyzed the degradation as a function of the oxide aperture in 845 nm VCSELs designed for silicon photonics (SiPh) applications. First, we evaluated the optical degradation of the devices by collecting EL images during a constant current stress. The experimental results showed an increased spreading of the optical beam of the VCSEL with increasing ageing time. Based on numerical simulations, we demonstrated that the electrical degradation (increase in series resistance) is responsible for a larger current spreading which, in turn, increases the FWHM (full width half maximum) of the optical beam. We further evaluated the series resistance variation by aging four lasers with different oxide apertures. The results of this set of experiments showed that the electrical degradation is stronger as the oxide aperture is smaller, and mostly depends on the contribution of the top DBR resistance. Thanks to our analysis we proved that the use of a larger aperture can result in a better device reliability.**

***Index Terms*—Degradation, VCSEL, Diffusion, Oxide aperture, PICs.**

Manuscript received 26 January 2024; revised 27 April 2024; accepted 13 June 2024. Date of publication 18 June 2024; date of current version 3 September 2024. *(Corresponding author: Michele Zenari.)*

Michele Zenari, Matteo Buffolo, Fabiana Rampazzo, Carlo De Santi, Gaudenzio Meneghesso, and Enrico Zanoni are with the Department of Information Engineering, University of Padova, 35131 Padova, Italy (e-mail: michele.zenari@dei.unipd.it; matteo.buffolo.1@unipd.it; rampazzo@dei.unipd.it; carlo.desanti@unipd.it; gauss@dei.unipd.it; zanoni@dei.unipd.it).

Francesca Rossi and Laura Lazzarini are with the IMEM, CNR Parma, 43124 Parma, Italy (e-mail: francesca.rossi@imem.cnr.it; laura.lazzarini@imem.cnr.it).

Jeroen Goyvaerts is with the LIGENTEC SA, EPFL Innovation Park Bâtiment L, 1024 Ecublens, Switzerland (e-mail: jeroen.goyvaerts@ligentec.com).

Alexander Grabowski is with the Photonics Laboratory, Department of Microtechnology and Nanoscience, Chalmers University of Technology, SE-412 96 Göteborg, Sweden (e-mail: alexander.grabowski@chalmers.se).

Johan S. Gustavsson and Anders Larsson are with the Photonics Laboratory, Department of Microtechnology and Nanoscience, Chalmers University of Technology, SE-412 96 Göteborg, Sweden (e-mail: jgustavsson@nvidia.com; alarsson@nvidia.com).

Roel Baets and Günther Roelkens are with the Photonics Research Group, Ghent University-imec, 9052 Gent, Belgium (e-mail: roel.baets@ugent.be; gunther.roelkens@ugent.be).

Matteo Meneghini is with the Department of Information Engineering, University of Padova, 35131 Padova, Italy, and also with the Department of Physics and Astronomy, University of Padova, 35131 Padova, Italy (e-mail: matteo.meneghini@unipd.it).

Color versions of one or more figures in this article are available at https://doi.org/10.1109/JSTQE.2024.3415674.

Digital Object Identifier 10.1109/JSTQE.2024.3415674

I. Introduction

OVER the last twenty years, the need for high-capacity and low-power optical links has boosted research and investments in several new technologies, such as silicon photonics (SiPh). Silicon photonics promises to improve the efficiency and speed of telecommunications by developing photonic integrated circuits (PICs) based on silicon [1]. These goals are predicted to be reached in the next decades by leveraging the standard CMOS processes to miniaturize optics and attain high volumes with low costs. Silicon photonics finds application in a variety of fields, including datacom and telecom applications [2], sensors [3], and light detection and ranging systems (LIDARs) [4]. However, one limiting factor to the widespread adoption of SiPh-based PICs is the lack of efficient light sources. Indeed, silicon and other indirect bandgap semiconductors are unsuitable to develop high-efficiency lasers. To avoid the worsening of crystalline quality resulting from the material mismatch between silicon and III-V materials [5], different kinds of integration processes have been demonstrated: bonding [6], flip-chipping [7], and ultimately micro-transfer printing [8]. A significant effort has been put into integrating III-V edge-emitting devices such as Fabry-Pérot (FP), Distributed Bragg Reflector (DBR), and Distributed Feedback (DFB) laser diodes onto photonic integrated platforms. All these lasers feature long planar cavities and relatively high threshold currents, in the range of 10 to 100 mA. To meet the requirements of data communications in terms of power consumption [9], the energy per bit must be reduced. Vertical-cavity surface-emitting lasers (VCSELs) represent the state-of-the art of lasers for high-speed transmission, especially in short-reach communication [10]. The benefits of VCSELs over other types of laser diodes include high throughput wafer-level testing, easy interface with optical fibers, and, most importantly, sub-mA threshold currents and high slope efficiencies, which make VCSELs excellent candidates as light sources for PICs.

With respect to our previous work [11], we further investigate the optical and electrical reliability of 845 nm VCSELs suitable for integration in SiN platforms for silicon photonics with a new set of experiments. Firstly, we studied the optical degradation

of the devices under test by monitoring the EL (electroluminescence) emission map during a constant current stress. Concerning the electrical properties, we analyzed four VCSELs differing from the oxide aperture diameter (respectively 4, 5, 6, and 7 μm): by means of current step stress experiments, we then studied the influence of the device aperture on the series resistance worsening. Based on numerical simulations, we demonstrated that the diffusion of compensating impurities is responsible for i) the increase in series resistance, ii) the variation of the preferential current path, and iii) the widening of the optical beam shape of the laser. Furthermore, by investigating and modeling the degradation kinetics on devices with different apertures, we further proved that iv) the series resistance variation strongly depends on the increase in the overall resistivity of the p-DBR, and v) this process is mitigated for larger oxide apertures.

II. Devices Under Test

The devices analyzed within this work are vertical-cavity surface-emitting lasers emitting at 845 nm. The structure, starting from the top, includes a Ti/Pt/Au disk-shaped p-contact that serves both as electrode and as a top reflector. The top DBR is p-doped with carbon and consists of 29 mirror pairs of $Al_{0.12}Ga_{0.88}As/Al_{0.90}Ga_{0.10}As$. At the bottom of the p-DBR, within the layer closest to the separate confinement heterostructure (SCH) region, a 30 nm $Al_{0.98}Ga_{0.02}As$-layer is included for the formation of an oxide aperture, about 4 μm wide, through selective wet oxidation. The presence of this aperture laterally confines the current, and consequently the optical mode to the center of the circular VCSEL structure. The active area of the laser is located below the aperture and consists of a 1 $-$ λ thick SCH and a multi-quantum-well (MQW) structure containing five 4 nm thick $In_{0.10}Ga_{0.90}As/Al_{0.37}Ga_{0.63}As$ QWs. The bottom DBR is n-doped and is composed of 23 mirror pairs of $Al_{0.12}Ga_{0.88}As/Al_{0.90}Ga_{0.10}As$. A Ni/Ge/Au n-contact is positioned a few DBR mirror pairs below the active volume. At the bottom of the n-DBR, a 527 nm $Al_{0.12}Ga_{0.88}As$ buffer layer is purposely included to tune the cavity length between the bottom DBR and the diffraction grating. Underneath this layer, a 4 nm GaAs layer serves as an etch stop layer with respect to an $In_{0.49}Ga_{0.51}P$ sacrificial layer, which is required for the micro-transfer-printing process. Further information regarding the device epitaxy, growth, and fabrication can be found in [12]. The devices are meant to be transferred onto a SiN platform, thus allowing the fabrication of vertical-cavity silicon-integrated lasers (VCSILs) [12]. For the purposes of this work, the VCSELs have been transferred onto a glass substrate to analyze the bottom-side optical emission of the lasers by means of EL measurements.

III. Methodology

Concerning the measurement of the optical degradation of the devices, we tested a representative VCSEL with 7 μm oxide aperture on wafer. The chip was placed onto a sapphire window in order to measure the optical beam from the bottom of the device through a CCD camera (pixel size 8x8 μm). The sample was aged and characterized at room temperature by means of a source meter. To evaluate the degradation kinetics as a function of time, the device was submitted to a constant-current stress experiment. The aging test was interrupted at different stages to evaluate the effects of device degradation by carrying out optical measurements (L-I) and by collecting EL maps. In this work, we analyze the results of a constant current stress test carried out at 10 mA ($\approx$ 26 kA/cm^2). The stress current density was chosen according to the results presented in our previous work [11] with the goal of being able to observe the degradation kinetics in a reasonable amount of time ($<$5 kmin).

Regarding the analysis of the electrical degradation, we submitted one representative VCSEL for each aperture size (4, 5, 6, and 7 μm) to a current step-stress experiment. In this aging test, the stress current was increased by 200 A/cm^2 every hour starting from 200 A/cm^2. After each stage of the step-stress, an electrical characterization was carried out. The temperature control was achieved through a TEC-controlled baseplate, whereas the electrical characterization was performed by means of a parameter analyzer.

The unaged and aged structures have been studied by Trasmission Electron Microscopy techniques. The samples have been cross-sectioned in selected regions by means of focused ion beam (FIB). The lamellae have been studied by High Angle Annular Dark Field-Scanning TEM (STEM-HAADF) in a Jeol 2200FS microscope. This imaging mode allows to detect the Z-contrast and to obtain maps of chemical composition by the Energy Dispersive X-Ray Spectroscopy (EDS).

IV. Optical Degradation

A. Experimental Analysis

During the constant current stress, the optical power was measured by integrating the intensity of the EL images recorded by a CCD camera at different bias levels. To monitor the shape of the optical emissions, we focused on the EL images below threshold at 200 μA ($\approx$ 260 A/cm^2): Figure 1(a) reports the L-I curves below threshold, whereas Fig. 1(b) shows the EL image acquired on the unaged sample.

From the measurement of the EL maps taken at 200 μA, we extrapolated the vertical and horizontal beam profiles as a function of the stress time. As expected from the L-I characteristics, the integral of the profile, proportional to the total OP emitted by the device, decreases during the stress experiment. However, the most crucial feature observed during this test was the variation of the FWHM (full width half maximum) of the beam shape. We extrapolated the FHWM by a Gaussian fit from both vertical and horizontal profiles (Fig. 2(b) and (c)). The two kinetics (Fig. 2(a)) have almost the same trend and show a two-phases degradation. During the first phase (0–100 min), the beam spreading is milder, whereas during the second one (t $>$100 min) the variation is more pronounced. Towards the end of the experiment, the FWHM seems to remain fixed, however the detected behavior may depend on the very-low SNR achievable during the last stages of the stress test.

This peculiar two-phases degradation has already been studied on similar devices before, with focus on the electro-optical data, rather than on the beam profile. Indeed, according to

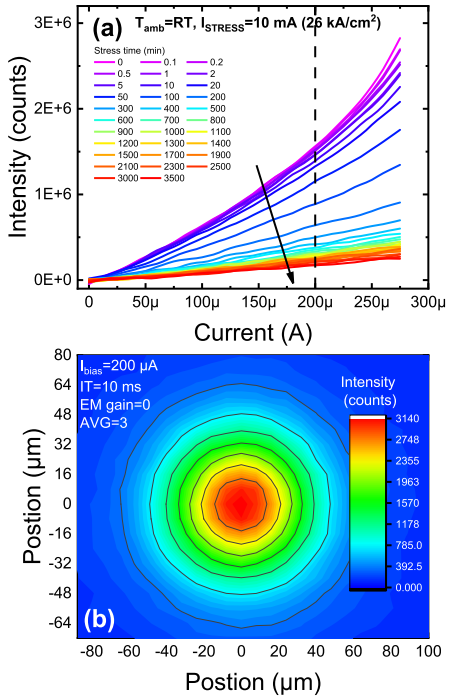

Fig. 1. (a) L-I characteristic below threshold: the vertical dashed line indicates the current level chosen for the beam profiling; the unaged device threshold current is $I_{th} = 300$ μA. (b) EL image acquired on the unaged device at 200 μA.

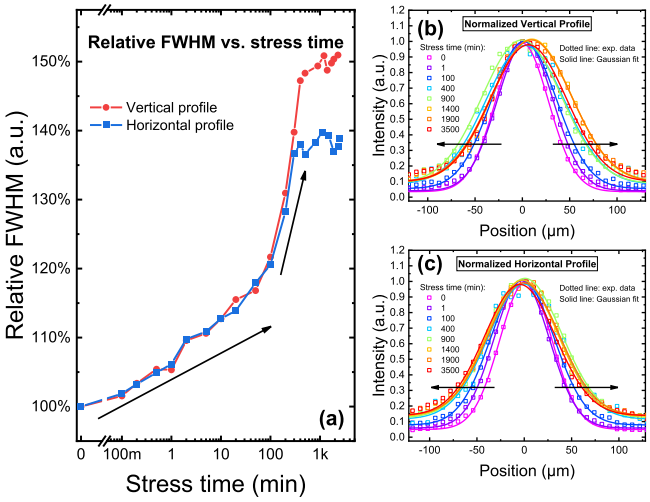

Fig. 2. (a) relative FWHM kinetics for horizontal and vertical profiles. (b) Normalized vertical profile (scatter) with superimposed Gaussian fit (solid). (c) Normalized horizontal profile (scatter) with superimposed Gaussian fit (solid).

[11], the degradation originates from the diffusion of impurities from the p-contact layers towards the active region. During the first phase of degradation, the impurities cross the top DBR worsening its optical and electrical performance of the lasers: this leads to an increment in both series resistance and threshold current [14]. During the second phase, on the other hand, the impurities start to reach the active region: in this condition the devices experience both a strong decrease in optical emission as well as a second series resistance increment. To relate our

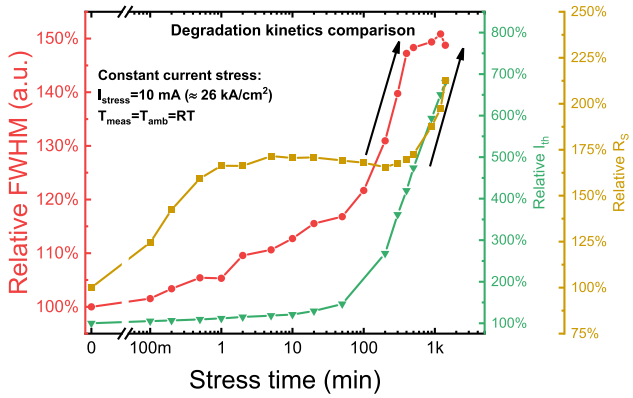

Fig. 3. Degradation kinetics comparison: threshold current (green) vs. series resistance (ocher) vs. FWHM (red).

previous findings with this new study, we compared the degradation kinetics of the FWHM (vertical profile) with the series resistance and threshold current kinetics. From Fig. 3 we can see that each of the three curves shows two clear phases. However, phase two of degradation for R_S and I_{th} starts around 200 min, whereas the beam profile starts to heavily spread at 100 min. According to our theory, the diffusion of impurity species is responsible for compensating the p-type dopants (carbon) in the top part of the device. Therefore, we suppose that the increment in series resistance in the device, due to the localized increase in resistivity, is responsible for spreading the current out from the center of the device (aperture). A schematic representation of the degradation process is represented in Fig. 4. Finally, this phenomenon results in the FWHM increase of the optical beam profile. Moreover, we observe that the second phase of degradation is anticipated for the FWHM with respect to the variation of I_{th} and R_S. To explain this phenomenon, we have to consider that the oxide aperture is responsible for confining the current, thus defining also the emission profile, and the impurities reach the oxide aperture before the active region. For these reasons, the second phase of degradation affects before the FHWM (strictly related to the aperture) and then the threshold current and the series resistance (related to the active layers).

B. TEM Analysis

The STEM-HAADF image of Fig. 5(a) shows the region of the 4 μm nominal diameter oxide aperture in an aged device, together with wide regions of both the top and the bottom DBR. Being a Z-contrast image, the bright stripes correspond to layers containing more Ga, while the darker ones contain more Al. The stripe in the middle of the picture with darkest sides corresponds to the oxide aperture. No extended defects are present neither in the imaged region nor in the other parts of the lamella. The careful inspection of the 'critical' oxide aperture region reveals that no extended defects are present as well. The spotty bright features are present in all the samples investigated, aged and unaged, and are more likely due to the thinning and polishing procedure. Figure 5(b) present higher magnification pictures of the aperture edges, red squared in a). It has been reported ([13]) that dislocations usually are present

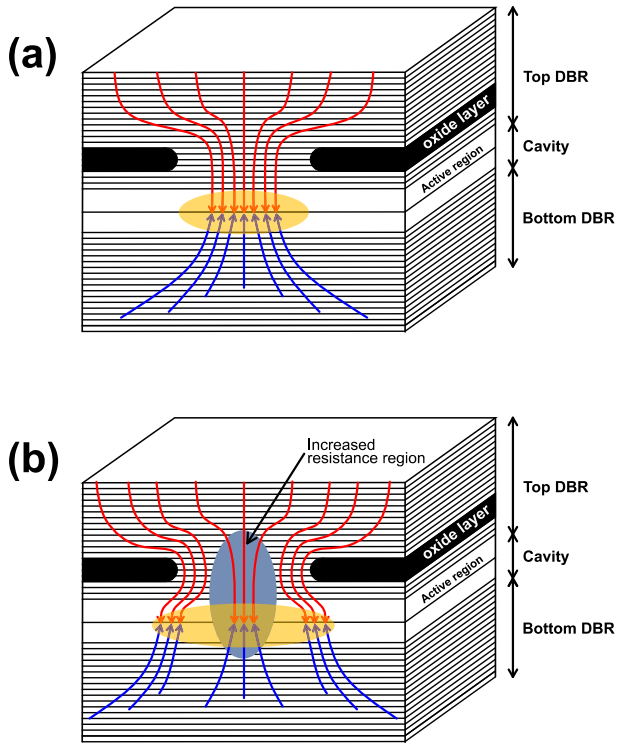

Fig. 4. Schematic representation of the degradation model. The blue curves represent the electron current lines whereas the red curves indicate the hole current lines. (a) unaged device, normal current density distribution; the yellow shape represents the region where coherent photons are emitted. (b) post-stress device, the diffusion of impurities increases the resistance in the middle of the structure causing a variation of the current density distribution. The emission region (yellow shape) becomes wider due to current redistribution.

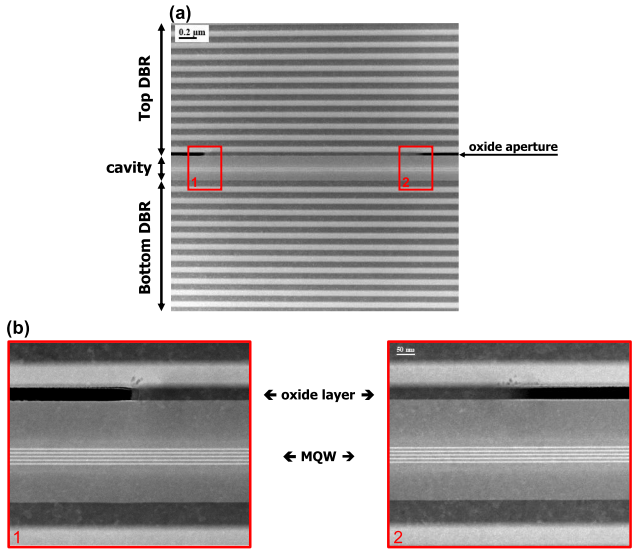

Fig. 5. STEM-HAADF images of an aged VCSEL. The device are not affected by extended defects neither in the DBRs (a) nor in the active region and/or in the oxide layer edges (b).

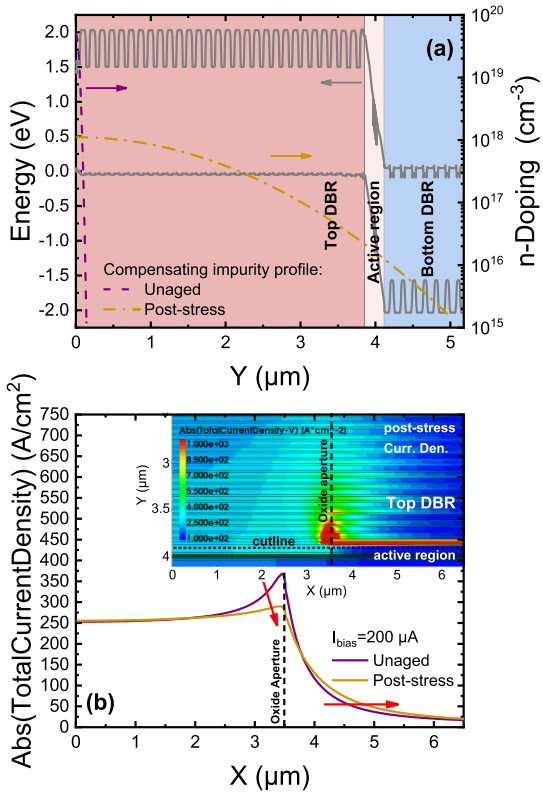

Fig. 6. (a) doping compensation profiles for unaged and post-stress conditions superimposed to the band diagram at equilibrium. (b) Variation of the absolute current density below the oxide aperture (200 μA); the inset shows the 2D current density distribution.

in these regions in aged devices. The dark small spots above the oxide layer edges correspond to voids, possibly induced by the manufacturing procedure. The EDS maps did not reveal any compositional inhomogeneities, at least within the detection limits of the technique. As for point defects, either vacancies or interstitials, they are detectable by TEM only if organized, forming extended defects. Isolated point defects do not have any clear effect on the image contrast, in our imaging conditions.

C. Simulation Analysis

To validate our conclusions regarding the variation of the optical beam profile, we simulated the current spreading in the device structure by a commercial Poisson-drift-diffusion simulator (Synopsis Sentaurus TCAD). Further information about the model employed for the simulations can be found in [14]. We simulated the current density spreading in the VCSEL by applying a Gaussian distribution of n-type compensating species in two distinct cases (see Fig. 6(a)). For the unaged device, the Gaussian distribution is placed close to the p-contact layers (peak $= 5{\cdot}10^{19}$ cm^{-3}, $\sigma = 30.5$ nm), whereas, for the post-stress device, the Gaussian distribution is located across the top DBR and the active region (peak $= 1.15{\cdot}10^{18}$ cm^{-3}, $\sigma = 1379$ nm): for a detailed description of the choice of parameters see Paragraph VII in [14]. From the outcome of the simulation, we investigated the absolute value of the current density vector, at a bias level of 200 μA, across the device structure (see the inset of Fig. 6(b)). In the post-stress condition, in particular below the oxide aperture, the current density lowers in the center of the device (i.e., within the oxide aperture) and spreads towards the lateral edges (Fig. 6(b)). This feature can be explained by

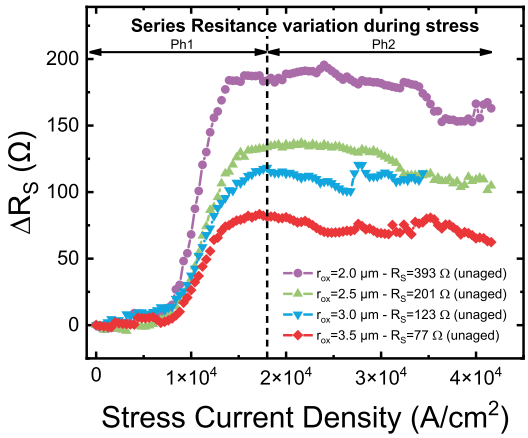

Fig. 7. Variation of series resistance as a function of stress current density, for four geometries: $r_{ox} = 2$, 2.5, 3, and 3.5 μm. The dashed vertical line indicates the end of the major series resistance variation.

considering that the compensating impurities are increasing the series resistance of the device as they are migrating towards the active region, due to the creation of potential barriers in the valence band edge in the top DBR (see Fig. 6(b) in [14]). This outcome further supports our previous reports, and points out that the electrical degradation (R_S increment) is in turn responsible for the worsening of the optical properties, i.e., the FWHM increment and intensity reduction of the EL, below threshold.

V. Electrical Degradation As a Function of the Oxide Aperture

A. Experimental Evidences

In the previous part, we evaluated how the electrical degradation (R_S increment) impacts the optical properties (spread of optical beam) of the devices under investigation. Considering that the overall series resistance of the device has a strong dependence on the oxide aperture (since it confines the current flow in the center of the device) and considering the strong correlation between the electrical and optical correlation of the devices, both below and above threshold, we decided to investigate how the width of oxide aperture affects the degradation of the devices, and, therefore which configuration improves the reliability. In this second analysis, we focus on the electrical degradation for four different VCSEL geometries (oxide apertures of 4, 5, 6, and 7 μm) via current step-stress experiments. The unaged devices have different initial series resistance because the oxide aperture is mostly responsible for current confinement. Indeed, the device with a larger aperture (7 μm) has an initial R_S of 77 Ω, whereas the smaller (4 μm diameter) has the highest series resistance, about 393 Ω. To fairly compare the degradation of the four samples, we evaluated the series resistance variation, with respect to the unaged R_S, as a function of the stress current density: Fig. 7 reports the four kinetics. During the first phase of degradation, Ph1, the devices show the major degradation around 10 kA/cm^2, finally reaching a plateau, sort of, after aging at $J_{stress} = 20$ kA/cm^2 where starts Ph2: remarkably, the narrower the oxide aperture is, the higher the observed variation is.

B. Modeling of Series Resistance Variation As a Function of the Oxide Aperture

To explain the dependence of the series resistance variation as a function of the oxide aperture, we modeled the overall series resistance of the VCSEL as the sum of two contributions, the oxide aperture series resistance (R_{ox}) and the top DBR resistance (R_{DBR}):

$$R_S = R_{ox} + R_{DBR} \tag{1}$$

We did not consider the contribution of the bottom DBR because we assumed that the majority of impurities is crossing the top DBR and the active region. Moreover, the n-side of the device becomes even larger than the mesa width, therefore its resistance contribution can be neglected (the lateral current density flows within a sheet of $\approx$ 150 nm below the mesa, according to our simulations). The resistance of the aperture can be expressed simply by considering Ohm's law:

$$R_{ox} = \rho_{ox} \frac{t_{ox}}{A_{ox}} \tag{2}$$

where ρ_{ox} is the resistivity of the oxide aperture, whereas t_{ox} and A_{ox} are respectively the oxide layer thickness and the area of the region limited by the oxide aperture. Concerning the resistance contribution of the top DBR we have:

$$R_{DBR} = \frac{\rho_{DBR}}{\pi} \frac{L}{\frac{r_{ox} W}{2}} \tag{3}$$

where ρ_{DBR} is the resistivity of the top DBR, r_{ox} is the radius of the oxide aperture, and W is the mesa width. A detailed description of the calculations of the top DBR resistance can be found in Appendix A. According to our degradation model, the impurities that migrate from the p-contact layers towards the active region increase the series resistance by compensating the p-dopant species. In a first-order approximation, this process can be modeled by a variation in the overall DBR resistivity (ρ_{DBR}), as the other geometrical parameters are supposed to be unaltered during the stress experiment. Since we are considering only the degradation during the first degradation phase (i.e., the major series resistance increment) we do not expect to have a large amount of impurities close to the oxide aperture. For this reason, we do not consider any variation in the oxide aperture resistance R_{ox}. Moreover, the impurities are expected to create potential barriers in the valence band (as we evaluated in [14]), so structural variation of oxide aperture is unlikely and was not experimentally reported so far. The series resistance variation, considered at the degradation stage indicated by the dashed line in Fig. 7, can be expressed as:

$$\begin{aligned} \Delta R_S &= R_S^{post} - R_S^{pre} \\ &= \frac{\rho'_{DBR}}{\pi} \frac{L}{\frac{r_{ox} W}{2}} + \rho_{ox} \frac{t_{ox}}{A_{ox}} \end{aligned}$$

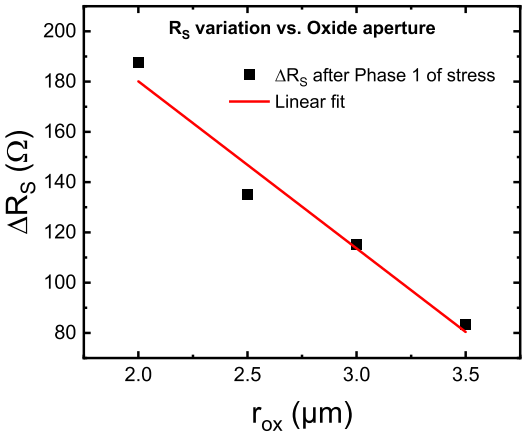

Fig. 8. Series resistance variation as a function of the oxide radius. The experimental data confirm the inverse proportionality (here fitted with a linear function as a first-order approximation) between the degradation and the aperture of the VCSEL.

$$-\left(\frac{\rho_{DBR}}{\pi}\frac{L}{\frac{r_{ox}W}{2}}+\rho_{ox}\frac{t_{ox}}{A_{ox}}\right)$$
$$=\frac{(\rho'_{DBR}-\rho_{DBR})}{\pi}\frac{L}{\frac{r_{ox}W}{2}} \quad (4)$$

where R_S^{post} represents the series resistance measured after the major series resistance degradation, and R_S^{pre} represents the unaged series resistance of the unaged device. ρ'_{DBR} is the resistivity of the DBR after aging. The resulting R_S variation is dependent on geometrical parameters, including the oxide radius r_{ox}, which is the only parameter changing between the four devices under investigation. Fig. 8 shows the approximately linear relation between ΔR_S and r_{ox}: which highlights that the devices with a larger aperture are characterized by a lower series resistance increment. Ultimately, this result indicates that the larger the aperture, the more the device is stable in terms of electrical degradation. Indeed, a large series resistance variation increases the electrical power consumption ($\propto RI^2$), thus resulting in a reduction of the power efficiency.

VI. Conclusion

In summary, we analyzed the reliability of 845 nm VCSELs for silicon photonics by means of two different aging experiments. Firstly, we studied the optical degradation of a 7 μm aperture VCSEL by leveraging the EL images collected during a constant current stress at 10 mA ($\approx$26 kA/cm^2). From the analysis of the sub-threshold EL map, we observed the spread of the FHWM of the emission profile during the stress experiment. By means of numerical simulations, we demonstrated that this behavior is fully compatible with the diffusion of compensating impurities which locally increase the resistance of the p-side of the devices, effectively shunting away the injected current from the central aperture, and thus inducing the observed spreading of the optical beam.

The role of the oxide aperture in the electrical degradation of the devices was further investigated by carrying out a series of current step-stress tests on devices differing only in the width of the oxide aperture. The experimental results showed that the series resistance variation is more pronounced for narrower oxide apertures. In particular, we found that the series resistance variation of the devices under investigation is inversely proportional to the radius of the oxide aperture, as indicated by the experimental data.

In conclusion, increasing the aperture size of the VCSEL improves the electrical reliability of the devices. Nonetheless, in the design process, other specifications are also considered such as the single mode operation and threshold current reduction (smaller aperture) indicating the necessity of a tradeoff between performance and reliability. From the results obtained within this work, it was possible to address the main reliability challenges of 850 nm VCSELs designed to be integrated into SiN platforms for silicon photonics applications. In addition, the findings of our study can be considered valid for any AlGaAs-based bottom-emitting VCSELs operating at 850 nm.

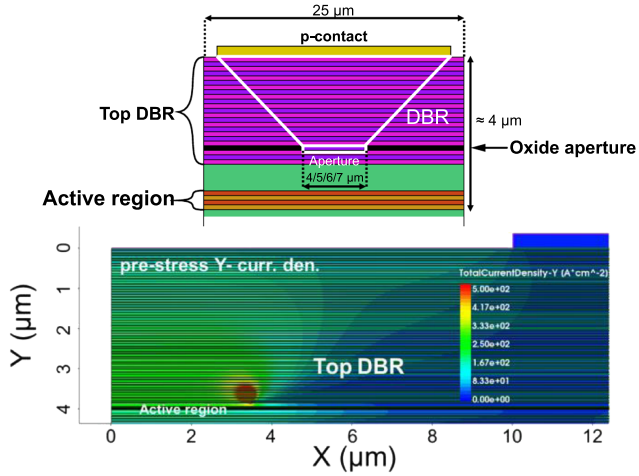

Fig. 9. The schematic above represents the upper part of the VCSEL and the two series resistance contributions (white polygons). The trapezoidal shape indicated for the DBR resistance is justified by Y component of the current density depicted in the image below (half VCSEL). The detailed modeling of the series resistance is defined in Appendix A.

Appendix A
Determination of DBR series resistance formula

To define the DBR contribution on the series resistance of the VCSEL we have to consider the preferential path of the current injected at the p-contact. We approximated the actual resistance contribution of the DBR by considering the current flow from the p-contact towards the oxide aperture forming a truncated cone (see the schematic of Fig. 9). Numerically, we defined the resistance of the entire DBR as a sum of infinitesimal circular disks of radius $r_{ox}+R_i$, where R_i is the generic distance between the oxide aperture and the edge of the cone, and thickness dh. To calculate R_i as a function of the heigh h, (i.e., the distance from the oxide layers to the generic infinitesimal disk of radius R_i, we followed the calculations depicted in Fig. 10):

The total resistance of the truncated cone, representing the path of the current flow, is the integral over the contribution of

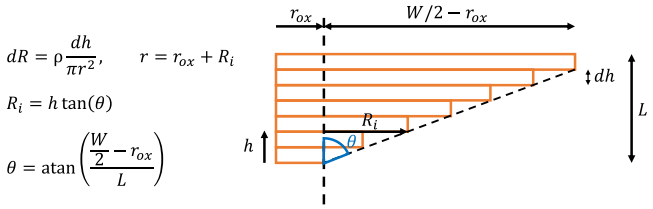

Fig. 10. Definition of the DBR resistance as the sum of infinitesimal disks contributions of radius $r_{ox}+R_i$ and thickness dh. W is the mesa width and L is the depth of the DBR.

each infinitesimal disk.

$$dR = \rho\frac{dh}{\pi r^2} = \rho\frac{dh}{\pi[r_{ox} + htan(\theta)]^2}$$

$$\Rightarrow R = \frac{\rho}{\pi}\int_0^L \frac{1}{[r_{ox} + htan(\theta)]^2}dh \tag{5}$$

the result of the last equation becomes:

$$= \frac{\rho}{\pi}\frac{1}{\tan(\theta)}\left.\frac{-1}{r_{ox} + htan(\theta)}\right|_{h=0}^{h=L}$$

$$= \frac{\rho}{\pi}\left(\frac{1}{tan(\theta)\, r_{ox}} - \frac{1}{tan(\theta)\,[r_{ox} + Ltan(\theta)]}\right) \tag{6}$$

Since $\theta = \text{atan}(\frac{\frac{W}{2} - r_{ox}}{L})$ we can write

$$= \frac{\rho}{\pi}\left\{\frac{1}{\left(\frac{\frac{W}{2} - r_{ox}}{L}\right) r_{ox}} - \frac{1}{\left(\frac{\frac{W}{2} - r_{ox}}{L}\right)\left[r_{ox} + L\left(\frac{\frac{W}{2} - r_{ox}}{L}\right)\right]}\right\}$$

$$= \frac{\rho L}{\pi}\left(\frac{\left(\frac{W}{2}\right)^2 - 2r_{ox}\frac{W}{2} + r_{ox}^2}{r_{ox}\frac{W}{2}\left(\frac{W}{2} - r_{ox}\right)^2}\right) \tag{7}$$

Recognizing that $(\frac{W}{2})^2 - 2r_{ox}\frac{W}{2} + r_{ox}^2$ is equal to $(\frac{W}{2} - r_{ox})^2$ (square of a binomial), we eventually obtain:

$$R = \frac{\rho}{\pi}\frac{L}{r_{ox}\frac{W}{2}} \tag{8}$$

REFERENCES

[1] S. Y. Siew et al., "Review of Silicon Photonics technology and platform development," *J. Lightw. Technol.*, vol. 39, no. 13, pp. 4374–4389, Jul. 2021, doi: 10.1109/JLT.2021.3066203.

[2] K. Ogawa et al., "Silicon Mach-Zehnder modulator of extinction ratio beyond 10dB at 10.0-12.5Gbps," *Opt. InfoBase Conf. Papers*, vol. 19, no. 26, pp. B26–B31, Dec. 2011, doi: 10.1364/oe.19.000b26.

[3] C. Dhote, A. Singh, and S. Kumar, "Silicon photonics sensors for biophotonic applications - A review," *IEEE Sens. J.*, vol. 22, no. 19, pp. 18228–18239, Oct. 2022, doi: 10.1109/JSEN.2022.3199663.

[4] X. Zhang, K. Kwon, J. Henriksson, J. Luo, and M. C. Wu, "A large-scale microelectromechanical-systems-based silicon photonics LiDAR," *Nature*, vol. 603, no. 7900, pp. 253–258, Mar. 2022, doi: 10.1038/s41586-022-04415-8.

[5] Q. Li and K. M. Lau, "Epitaxial growth of highly mismatched III-V materials on (001) silicon for electronics and optoelectronics," *Prog. Cryst. Growth Characterization Mater.*, vol. 63, no. 4, pp. 105–120, 2017, doi: 10.1016/j.pcrysgrow.2017.10.001.

[6] A. W. Fang et al., "Electrically pumped hybrid AlGaInAs-silicon evanescent laser," *Opt. Exp.*, vol. 14, no. 20, pp. 9203, Oct. 2006, doi: 10.1364/oe.14.009203.

[7] A. Moscoso-Mártir et al., "Hybrid silicon photonics flip-chip laser integration with vertical self-alignment," in *Proc. Conf. Lasers Electro-Opt. Pacific Rim*, Nov. 2017, pp. 1–4, doi: 10.1109/CLEOPR.2017.8118971.

[8] J. Zhang et al., "III-V-on-Si photonic integrated circuits realized using micro-transfer-printing," *APL Photon.*, vol. 4, no. 11, Nov. 2019, Art. no. 110803, doi: 10.1063/1.5120004.

[9] A. Malik et al., "Low power consumption silicon photonics datacenter interconnects enabled by a parallel architecture," in *Proc. Opt. Fiber Commun. Conf. Exhib.*, 2021, pp. 1–3, doi: 10.1364/ofc.2021.w6a.3.

[10] S. Kumari et al., "Vertical-cavity silicon-integrated laser with In-plane waveguide emission at 850 nm," *Laser Photon. Rev.*, vol. 12, no. 2, pp. 1–7, 2018, doi: 10.1002/lpor.201700206.

[11] M. Zenari et al., "Understanding the optical degradation of 845nm micro-transfer-printed VCSILs for photonic integrated circuits," *IEEE J. Quantum Electron.*, vol. 59, no. 4, Aug. 2023, Art. no. 2400210, doi: 10.1109/JQE.2023.3283514.

[12] J. Goyvaerts et al., "Enabling VCSEL-on-silicon nitride photonic integrated circuits with micro-transfer-printing," *Optica*, vol. 8, no. 12, 2021, Art. no. 1573, doi: 10.1364/optica.441636.

[13] R. W. Herrick et al., "Corrosion-based failure of oxide-aperture VCSELs," *IEEE J. Quantum Electron.*, vol. 49, no. 12, pp. 1045–1052, Dec. 2013, doi: 10.1109/JQE.2013.2285572.

[14] M. Zenari et al., "Modeling the electrical degradation of micro-transfer printed 845 nm VCSILs for silicon photonics," *IEEE Trans. Electron Devices*, vol. 71, no. 2, pp. 1–8, Feb. 2024, doi: 10.1109/TED.2023.3346370.

Michele Zenari was born in Soave (VR), Italy, in 1996. He received the master's degree in electronic engineering with a thesis on the analysis and modeling of InAs Quantum Dot lasers epitaxially grown on silicon in 2020 from the University of Padua, Padua, Italy, where he has been working toward the Ph.D. degree in information and communication science and technology with the Department of Information Engineering since 2020. He is working on the characterization and reliability of quantum dot lasers and vertical-cavity surface-emitting lasers for silicon photonics with the University of Padua.

Matteo Buffolo (Member, IEEE) was born in Vittorio Veneto, Italy, in 1986. He received the master's degree in electronic engineering with a thesis focusing on the analysis of the degradation mechanisms of GaN-based mid-power white LEDs from the University of Padova, Padua, Italy, and the Ph.D. degree from the Department of Information Engineering, University of Padova, in 2018. He is currently a Postdoc with the University of Padova. His research interests include the reliability of lighting systems employing GaN-based devices (lasers and LEDs) and investigation of the degradation mechanisms that affect modern IR laser sources for integrated telecommunication applications.

Fabiana Rampazzo received the degree in physics from the University of Padova, Padua, Italy, in 2001, and the Ph.D. degree in electronics and telecommunications engineering with a thesis entitled " Current instabilities, passivation effects and other reliability aspects in AlGaN/GaN HEMTs for Microwave applications" in 2005. She is currently a Laboratory Assistant with the University of Padova. She is working on characterization and reliability of M.O.S. capacitors with Silicon Carbide substrate. Her research interests include the characterization of microwave devices on III-V semiconductors such as GaN, GaAs, and InP, with particular aim to transient phenomena, electrical characterization of electronic devices grown on wide bandgap semiconductors (SiC and GaN), reliability studies of the long term stability of microwave devices with particular attention to their failure mode and mechanisms with also the help of S.E.M, and F.I.B. She was involved in many European Projects concerning GaN HEMTs reliability such as Korrigan, Euganic, Relgan, 5GGan2, AlInWon, E2coGaN, ErG, and Hiposwitch.

Carlo De Santi (Member, IEEE) was born in Verona, Italy, in 1985. He received the Ph.D. degree in 2014. He is currently a Postdoc with the Microelectronics Group, University of Padova, Padua, Italy. He is the author of more than 30 peer-reviewed journal papers, 50 contributions in conference proceedings, and four book chapters. His research interests include characterization, physical modeling, and reliability of various GaN-,GaAs-, InP-, Ga2O3-, CdTe- and Si-based electronic, and optoelectronic devices.

Francesca Rossi received the M.S. degree in physics and the Ph.D. degree in materials science from the University of Parma, Parma, Italy. She is currently a Senior Researcher with the Italian National Research Council and works with the Institute of Materials for Electronics and Magnetism, Parma, where she is the coordinator of the Structural and Surface Characterisation research activity. Her research interests include the analysis of advanced multifunctional hetero-structures based on thin films, QWs, QDs, 2D flakes or nanowires for energetic, sensor, micro-, and opto-electronic applications. She carries out scanning and transmission electron microscopy, cathodoluminescence and El electroluminescence, and X-Ray diffraction analyses to study structural properties and extended defects, carrier confinement in quantum structures, charge transport and injection mechanisms in the active region of devices, internal or applied electric field effects, and role of point defects and related complexes in doped layers and devices.

Laura Lazzarini is currently a Physicist, research director with CNR-IMEM with more than 35 years of experience in materials science characterization, mainly in transmission and scanning electron microscopy, and cathodoluminescence applied to both massive semiconductor materials and low-dimensional structures. She studied the role of strain in the generation of extended defects in structures with lattice mismatch, developing some models that have led to the creation of balanced strain structures for optical modulators and very high efficiency photovoltaic cells. She also studied the correlation between the structural and optical properties of materials and their impact on applications. She is most dedicated to the methodological development and application of advanced high-resolution analytical microscopy techniques for the study of nanostructured material systems for energy, opto- and nano-electronics, photonics, catalysis, sensing, and delivery of drugs. She coauthored more than 170 papers in ISI journals (GS h index $= 32$), seven book chapters, one review for Encyclopedia, and presented more than 160 contributions in international conferences (seven invited, two awards). She has been the IMEM person in charge for national and EU projects and EU expert evaluator. She is also a Supervisor of Ph.D. degree and master degree's Theses and teaches with the Ph.D. School of Materials Science and Technology, Parma University, Parma, Italy.

Jeroen Goyvaerts received the M.Sc. degrees in nanoscience and nanotechnology from the Catholic University of Leuven, Leuven, Belgium, and in photonics from the Polytechnic University of Catalunya, Barcelona, Spain, and the Ph.D. degree from the Department of Information Technology, Ghent University, Ghent, Belgium, in 2021, for his work on integrating GaAs opto-electronic components onto SiN waveguide circuits by means of micro-transfer-printing. Since 2021, he has been with the LIGENTEC SA team as a Design Engineer and Project leader, to further commercialise low-loss SiN waveguide technology for applications in computing, metrology, and sensing.

Alexander Grabowski received the M.Sc. degree in electrical engineering and the Ph.D. degree from the Chalmers University of Technology, Göteborg, Sweden, in 2017 and 2022, respectively. He is currently a Postdoc with the Department of Microtechnology and Nanoscience, Chalmers. He has worked on GaAs-based vertical-cavity surface-emitting lasers (VCSELs) in high-speed short-reach optical interconnects, mainly focusing on modeling of the VCSEL. He has also done work on fabrication of GaAs-based VCSELs for micro-transfer-printing integration on a silicon nitride PIC platform.

Johan S. Gustavsson received the M.Sc. degree in electrical engineering and the Ph.D. degree in photonics from the Chalmers University of Technology, Gothenburg, Sweden, in 1998 and 2003, respectively. His Ph.D. thesis was focused on mode dynamics and noise in vertical-cavity surface-emitting lasers (VCSELs). Since 2003, he has been a Researcher with the Photonics Laboratory, Chalmers, with an Assistant Professor position from 2004 to 2008, and an Associate Professor position since 2011. From September to October 2009, he was a Visiting Scientist with CNR Polytechnico, Turin, Italy. In 2016, he co-founded the spin-off company OptiGOT AB, which was acquired by Nvidia Corporation in 2020. In 2017, he co-organized the European Semiconductor Laser Workshop in Copenhagen. He has authored or coauthored more than 250 scientific journals and conference papers and two book chapters. His research interests include semiconductor lasers for short to medium reach communication and sensing applications. This has included surface relief techniques for mode and polarization control in VCSELs, 1.3 μm InGaAs VCSELs/GaInNAs ridge waveguide lasers for access networks, 2.3–3.5 μm GaSb VCSELs for CO, CO_2, and NH_3 sensing, and tunable VCSELs via moveable mirror for reconfigurable optical interconnects. He is currently working on energy efficient 56 Gbaud GaAs-based VCSELs for next generation datacom links, UV/blue AlGaN/GaN VCSELs for sterilizing/illumination, high contrast gratings as feedback/wavelength setting/focusing elements in micro-cavity lasers, and heterogeneous integration of III/V-based VCSEL material on a Si platform. He is also exploring photon-photon resonance effects to boost the modulation bandwidth in GaAs-based VCSELs.

Roel Baets (Life Fellow, IEEE) is currently a full Professor with Ghent University, Ghent, Belgium, where he leads a mixed UGent – imec team. For about 40 years Roel Baets has worked in the field of integrated photonics, in multiple material platforms (silicon, silicon nitride, III-V). He has made diverse scientific contributions to this field, as well as to its applications and spin-off creation in telecom, datacom, and sensing. He has led major research projects in silicon photonics in Europe and founded ePIXfab, the globally first Multi-Project-Wafer service for silicon photonics and the European Silicon Photonics Alliance. His research focuses on medical and environmental sensing applications of silicon photonics. He is a Fellow of European Optical Society and Optical Society. He was the recipient of the 2018 PIC-International Lifetime Achievement Award and 2020 John Tyndall Award.

Anders Larsson (Life Fellow, IEEE) received the M.Sc. and Ph.D. degrees in electrical engineering from the Chalmers University of Technology, Göteborg, Sweden, in 1982 and 1987, respectively. In 1991, he joined the faculty at Chalmers where he was promoted to Professor in 1994. From 1984 to 1985, he was with the Department of Applied Physics, California Institute of Technology, Pasadena, CA, USA. From 1988 to 1991, he was with the Jet Propulsion Laboratory, Pasadena. He has been a Guest Professor with Ulm University Ulm, Germany, Optical Science Center, University of Arizona at Tucson,Tucson, AZ, USA, Osaka University, Osaka, Japan, and Institute of Semiconductors, Chinese Academy of Sciences, Beijing, China. He has authored or coauthored close to 600 scientific journal and conference papers and two book chapters. His research interests include vertical-cavity surface-emitting lasers and optical interconnects. He co-organized the IEEE Semiconductor Laser Workshop 2004, organized the European Semiconductor Laser Workshop 2004, was a co-program Chair of European Conference on Optical Communication 2004, and the program and general Chair of IEEE International Semiconductor Laser Conference in 2006 and 2008, respectively. He was a Member of the IEEE Photonics Society Board of Governors during 2014–2016, an Associate Editor for IEEE/OSA JOURNAL OF LIGHTWAVE TECHNOLOGY during 2011–2016, and a Member of the editorial board of *IET Optoelectronics* during 2007–2020. In 2016, he co-founded OptiGOT AB, which was acquired by Nvidia in 2020. He has part-time positions with Chalmers and Nvidia. His scientific background is in the areas of optoelectronic materials and devices for optical communication, information processing, and sensing. He is a Fellow of OSA and EOS. In 2012, he was the recipient of the HP Labs Research Innovation Award.

Günther Roelkens (Senior Member, IEEE) received the degree in electrical engineering from Ghent University, Ghent, Belgium, in 2022, and the Ph.D. degree from the Department of Information Technology (INTEC), Ghent University in 2007. He is currently a full Professor with the Department of Information Technology (INTEC). In 2008, he was a visiting Scientist in IBM TJ Watson Research Center, New York. His research interests include the heterogeneous integration of III-V semiconductors and other materials on top of silicon waveguide circuits and electronic/photonic co-integration. He was holder of an ERC staring grant (MIRACLE), to start up research in the field of integrated mid-infrared photonic integrated circuit.

Gaudenzio Meneghesso (Fellow, IEEE) received the graduation degree in electronics engineering from the University of Padova, Padua, Italy, in 1992. He is working on the failure mechanism induced by hot-electrons in MESFETs and HEMTs. Since 2011, he has been a Full Professor with the University of Padova. He has authored or coauthored more than 800 technical papers, of which more than 100 invited papers in his research areas, which include electrical characterization, modeling, and reliability of microelectronics devices. He was nominated to IEEE Fellow class 2013, with the following citation, for contributions to the reliability physics of compound semiconductors devices. He was the recipient of the 12 Best Paper awards for his authored or coauthored papers.

Enrico Zanoni (Life Fellow, IEEE) was born in Verona, Italy, in 1956. He received the Laurea (*cum laude*) degree in physics from the University of Modena and Reggio Emilia, Modena, Italy, in 1982. Since 1997, he has been a Full Professor of digital electronics with the Department of Information Engineering, University of Padua, Padua, Italy.

Matteo Meneghini (Senior Member, IEEE) received the Ph.D. degree from the University of Padua, Padua, Italy, in 2008. He is currently an Associate Professor with the Department of Information Engineering, University of Padua, where he is involved in the electro-optical characterization and modeling of the performance and reliability of LEDs, lasers, HEMTs, and advanced solar cells.

Open Access funding provided by 'Università degli Studi di Padova' within the CRUI CARE Agreement